Materials Research Proceedings 28 (2023) 695-704 https://doi.org/10.21741/9781644902479-75

Total strain on the outer surface of steel sheets in air bending

POKKA Aki-Petteri[1,a *], KESTI Vili[2,b] and KAIJALAINEN Antti[1,c]

[1]University of Oulu, Materials and Mechanical Engineering, P.O. Box 4200, 90014 Oulu, Finland

[2]SSAB Europe, Rautaruukintie 115, 92101 Raahe, Finland

[a]aki-petteri.pokka@oulu.fi, [b]vili.kesti@ssab.com, [c]antti.kaijalainen@oulu.fi

Keywords: Air Bending, Steel, Digital Image Correlation, Strain Distribution, Total Strain, Bend Shape

Abstract. Air bending is a commonly used method for sheet-metal forming. However, several challenges exist around the bending behavior of materials with poor global formability, that are difficult to study using conventional bending test methods, and thus may not be fully understood. In this study, nine thermomechanically rolled steel grades with various strengths and ductility properties are bent using three different punch radii. The strain distributions on the outer surface are measured using Digital Image Correlation (DIC). The relationships between the strain distribution, peak strain, and total strain (area under the strain distribution curve) are determined. The total strain is observed to be independent from the peak strain and the shape of the strain distribution. The total strain is found to depend on the bend angle and sheet thickness. An analytical formula for approximating the total strain is derived. Potential for further approximations of the total strain, strain distribution and bend shape are discussed.

Introduction

Air bending is a commonly used forming method for sheet metals due to its flexibility, cost-effectiveness, and speed. A large range of bend angles can be achieved without tool changes just by controlling the punch displacement. The radius of the bent sheet is usually controlled by changing the punch radius. However, the shape of the bend is also dependent on the material properties. The distribution of strain and curvature on the outside bend surface can vary significantly depending on the work-hardening properties of the material. When bending materials with poor global formability (i.e., low work-hardening and uniform elongation), the inside radius of the bent sheet may decrease far below the punch radius, leading to high local strains and bend shapes that may be difficult to predict [1]. Various terms have been used referring to this phenomenon in previous studies: multi-breakage, gap formation, punch-sheet separation, punch detachment, punch-sheet-liftoff, loss of contact with the punch/sheet etc. [2-8]. The phenomenon has been known for a long time. However, research on the root of the phenomenon, i.e., the causes and effects of the strain distribution development in air bending, has been relatively scarce. Strain distributions in air bending have been studied by several authors [1,9-14], but not for a large selection of materials and punch radii, that would allow thorough analysis of the effects of certain tool parameters and material properties. Research in this area is therefore necessary.

In this paper, nine steel grades are bent in a 3-point bending setup using three different punch radii. The development of the strain distribution on the outer curvature is measured from each test using a Lavision Digital Image Correlation (DIC) system. The aim of the paper is to study the relationships between the strain distributions, peak strains, and total strains (area under the strain distribution curve).

Experimental Procedure

Nine thermomechanically rolled steel grades are tested in this study. Table 1 provides the sheet thicknesses, tensile properties of the investigated materials, along with the typical minimum bend radii for corresponding grades, provided by a steel manufacturer. The tensile data was measured from ISO 6892 compliant tests, using dog-bone specimens with straight sections of 6 × 8 × 45 mm^3, and strain rates of 0.0025 1/s (to yield point) and 0.008 1/s (after yield point). Both longitudinal and transverse directions were tested, relative to the material's rolling direction. In terms of the direction of the major strains relative to the rolling direction, the longitudinal (0°) tensile test corresponds to the transverse (TD) bend test and the transverse (90°) tensile test corresponds to the longitudinal (RD) bend test.

Table 1. Sheet thicknesses (t) and mechanical properties of the tested materials. The yield strength (R_e), ultimate tensile strength (R_m), uniform elongation (A_g) and total elongation with 40 mm gage length (A_{40}) were measured from the performed tensile tests. The minimum bend radii to 90° bend angle (R_{min}) were provided by a steel manufacturer for corresponding grades.

Material	t [mm]	R_e [MPa]	R_m [MPa]	A_g [%]	A_{40} [%]	R_{min} (to 90°)
St355 (0°/90°)	5.94	438/480	496/502	16.4/15.4	32.7/31.2	0.3 t
St500 (0°/90°)	5.92	585/628	653/669	11.7/10.4	26.9/25.4	0.8 t
St700 (0°/90°)	6.04	785/818	864/907	6.0/4.5	18.2/15.2	1 t
St900_1 (0°/90°)	5.99	974/1024	1042/1142	3.2/2.2	13.4/8.2	3 t
St900_2 (0°/90°)	5.93	1034/1067	1130/1151	3.9/3.1	13.9/11.4	3.5 t
St1100_1 (0°/90°)	6.01	1132/1127	1161/1172	4.7/4.7	15.4/13.8	3.5 t
St1100_2 (0°/90°)	5.93	1098/1111	1253/1271	2.9/2.4	12.1/10.8	3 t / 4 t
St1500 (0°/90°)	5.68	1537/1500	1761/1780	3.4/3.1	10.6/9.4	6 t
St1700 (0°/90°)	6.09	1740/1680	1958/1975	2.7/2.7	9.6/9.0	6 t

The bending tests are conducted in both longitudinal (RD) and transverse (TD) orientations. In this paper, the longitudinal bend orientation (RD) refers to the bend axis being parallel to the rolling direction, and the transverse orientation (TD) refers to the bend axis being perpendicular to the rolling direction. The bend specimens were cut from the 6 mm thick sheets into rectangular strips with a width of 80 mm. The specimen width is small enough to prevent exceeding the force limit of the used Zwick 100 kN universal tensile test machine, while still ensuring plane strain conditions at the center of the bend.

The specimens were bent in room temperature using purpose-built bending tools, shown in Fig. 1a. Using the tensile test machine for the bend tests allows accurate measurements of the bending force and punch displacement. The punch displacement is then used for calculating the bend angle according to ISO 7438 [15]. The measured vertical force is used to adjust the punch displacement and bend angle calculations for the vertical elasticity of the setup (51.9 kN/mm).

The shape of the die (lower bend tool) is illustrated in Fig. 1b. The openings allow an unobstructed line-of-sight between the DIC cameras and the measured specimen surface. The die width, i.e., the distance between the centers of the two shoulders, is also adjustable with this tool. The shoulders rotate freely in their sockets. To minimize the effect of friction even further, a PTFE lubricant spray is applied to the shoulders before each test.

Fig. 2 shows a schematic representation of the bending geometry used in this paper. Three bending tool setups are used in this study, in order to achieve a large variety of strain distributions, and to observe their effects on the behavior of the materials. The parameters for each setup are presented in Table 2. In each setup, the specimens were bent until they either fractured or reached the bend angle of α_{end}. Two repeat tests were conducted for each combination of tool setup, material, and bend orientation. Therefore, a total number of 108 tests are included in this study.

A DIC system, Strainmaster by Lavision, was used in this study for measuring the deformations on the outer bend surface. The system was equipped with two monochrome CCD cameras with a resolution of 2456 × 2058 pixels. The captured images were processed in the DaVis 8.4 software, which uses an iterative least squares matching (LSM) algorithm for displacement and strain calculation. The DIC recording and processing parameters are presented in Table 3. After calculating the strain maps from each image of each test, the values of the major strain were extracted from three sections positioned at the center of the bend, as illustrated in Fig. 1c. The average of the peak values of the three sections were also calculated at each point in time, as well as the average total strain (Riemann sums) of the three sections.

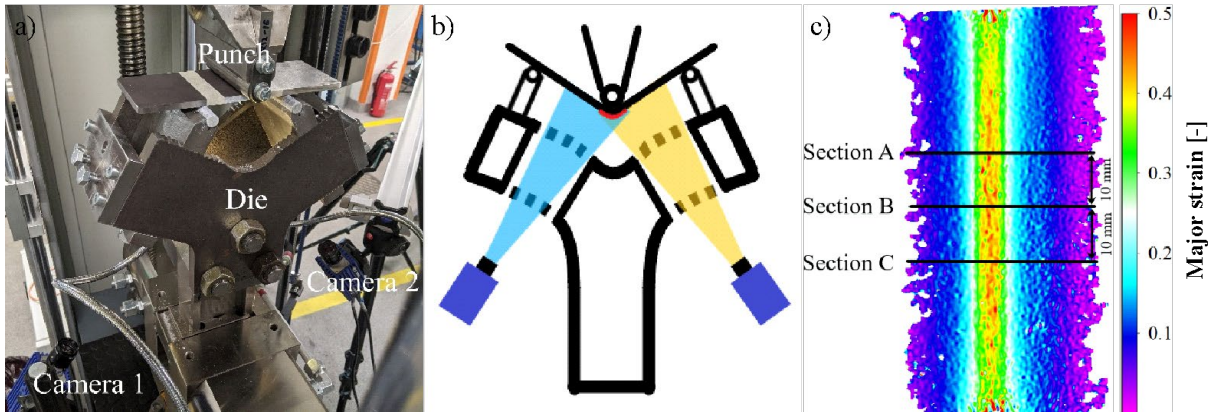

Fig. 1. a) The bending test setup, b) positioning of the DIC cameras, and c) sections A – C on a strain map of the St1100_1 (RD) at 90° bend angle, using a punch radius R_p = 2 t.

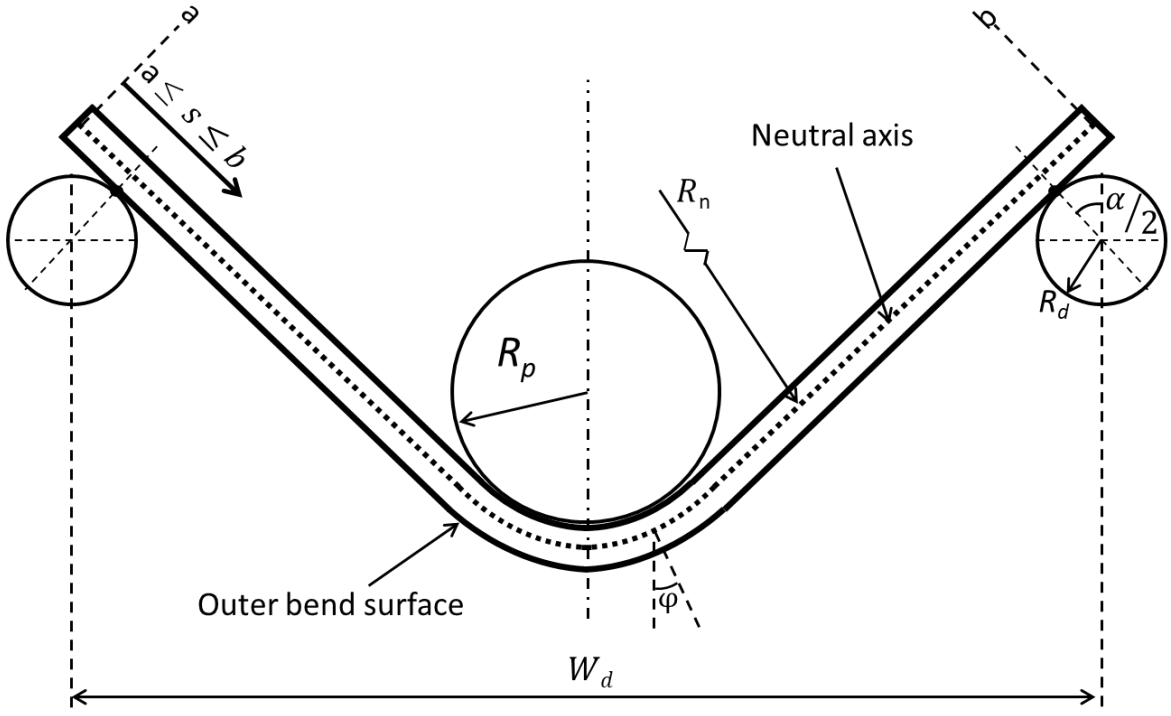

Fig. 2. The bending tool geometry and parameters involved in the analytical solution for the total strain $A_{\varepsilon b}$.

Table 2. Bending tool setup parameters: Punch radius (R_p), die width (W_d), radius of the die shoulders (R_d), vertical speed of the punch (V_p) and the final bend angle before unloading (α_{end}).

Tool setup	R_p	W_d [mm]	R_d [mm]	V_p [mm/s]	α_{end} [°]
1	4 mm ≈ 0.66 t	90	6	1	120
2	12 mm ≈ 2 t	90	6	1	100
3	24 mm ≈ 4 t	110	6	1	110

Table 3. Recording and processing parameters for the DIC system.

DIC system	Lavision Strainmaster (Stereo DIC)
Sensor and digitization	2456 × 2058, 12-bit
Lens, imaging distance	35 mm C-mount, 0.37 – 0.57 m
Imaging rate	2 Hz
Subset size	15x15 pixels
Step size	5 pixels
Strain window, smoothing method	5x5 data points, 2nd order polynomial fit
Virtual strain gage size	35 pixels
Image scale	21 – 30 pixels/mm
St.dev of principle strain	450 - 1700 microstrain
Interpolation, shape function, algorithms	6th order spline interpolation; affine shape function; LSM (iterative least squares matching) algorithm based on optical flow estimation

Before each test, a black-and-white speckle pattern was spray painted on the specimen surfaces to improve the DIC measurement reliability and to minimize glare. To minimize the effect of paint peeling on the measurements, the surfaces were cleaned with ethanol before painting and the tests were conducted as soon as possible after painting to prevent the paint from becoming excessively dry and brittle.

Results and Discussion

Fig. 3 shows the strain distributions of St700 in the RD direction measured at 30°, 60° and 90° bend angles and with three different punch radii. Fig. 3b illustrates the area under the strain distribution curve at 30°, i.e., the total strain $A_{\varepsilon b}$, as well as the peak strains ε_{b_max} at 30° and 90° angles. The distributions are similar for all three punches at 30° but as the bend angle increases, the effect of the punch radius on the strain distribution is clear. With the punch radius R_p = 0.66 t, the deformation increases mostly at the center, creating a narrow strain distribution with large peak strain at the center. In contrast, when using larger punches, as in Figs. 3b and 3c, the deformation is spread more evenly, creating a wider strain distribution with lower peak strains at the center. In fact, when using the largest punch (R_p = 4 t), the peak strain does not increase at all between 60° and 90° bend angles, as the deformation increases solely from the sides.

Fig. 4a presents the developments of the peak strain ε_{b_max} (average peak values of sections A, B and C) for St355 (TD) and St700 (RD) using three different punches. The peak strains develop almost identically in the first 15°, but after around 15 – 20° bend angle (0.05 – 0.10 peak strain) the effects of the punch radii and the material properties start to show. With the smallest punch radius (R_p = 0.66 t), the peak strain increases almost linearly between 30 – 90° bend angles for both materials, with only a slight stagnation in peak strain towards the end of the test. For R_p = 2 t, the stagnation of peak strain seems to start at around 30 – 40° bend angle, and for R_p = 4 t, around 15 – 20° bend angle.

The differences in material properties can also be seen in Fig. 4a. St355 produces lower peak strains than St700 with all three punches. This is due to the greater strain-hardening and ductility

of St355 compared to St700, indicated by their values of A_g and A_{40} in Table 1. In general, materials with greater work-hardening have greater resistance to strain localization, which leads to wider strain distributions and lower peak strains in bending.

Fig. 4b presents the developments of the total strain $A_{\varepsilon b}$ for St355 and St700. The total strain $A_{\varepsilon b}$ was calculated as the average of the Riemann sums of the strains in sections A, B and C shown in Fig. 1c. For clarification, the total strain $A_{\varepsilon b}$ represents the area under the strain distribution curve, as illustrated in Fig. 3b, and could also be described as the difference in length between the outer surface and the neutral axis. As can be seen in Figs. 4a and 4b, the total strain seems to grow at a similar, constant rate in all six tests, despite the differences in the peak strain development. The linear growth of the total strain continues until around 80°, after which some stagnation can be seen for all curves. It is assumed, that the apparent stagnation is mostly caused by loss of data at the later stages of the test, due to parts of the measured surface going beyond the field-of-view of the DIC cameras due to increased curvature. This can be seen in Figs. 3b and 3c, where the distributions at 90° angle are "cut off" at the edges, meaning that the increase of strain at the edges could not be fully measured. As the strain distribution is wider when using a larger punch, more data is lost at the edges with larger punches compared to smaller punches.

The peak strains and total strains from all tests at 50° and 80° angles are presented in Fig. 5. Despite the large number of tests and the variety in the peak strain values, no correlation between the total strain and peak strain or punch radius can be seen. At any given bend angle, the total bend strain value seems to be roughly constant, regardless of the peak strain or punch radius.

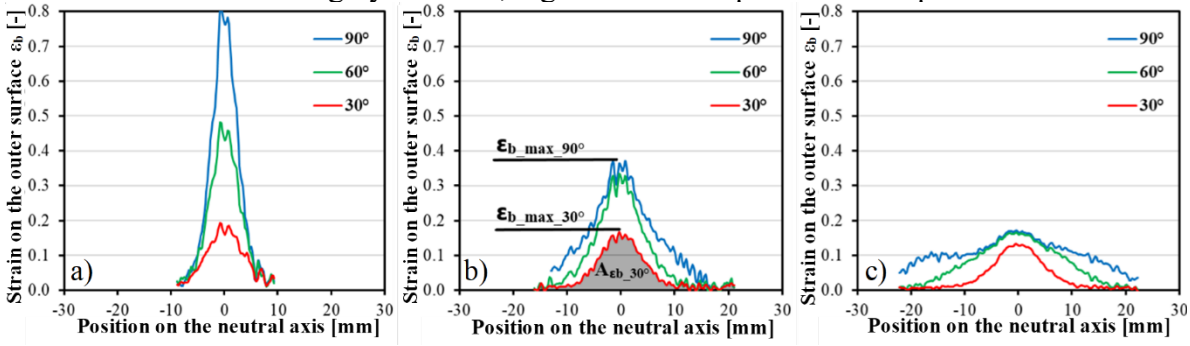

Fig. 3. Strain distributions at 30°, 60° and 90° bend angle, extracted from section B of St700 in the longitudinal direction (RD), using a punch radius of a) R_p = 0.66 t, b) R_p = 2 t and c) R_p = 4 t. The position on the neutral axis corresponds to a value of the arc coordinate s.

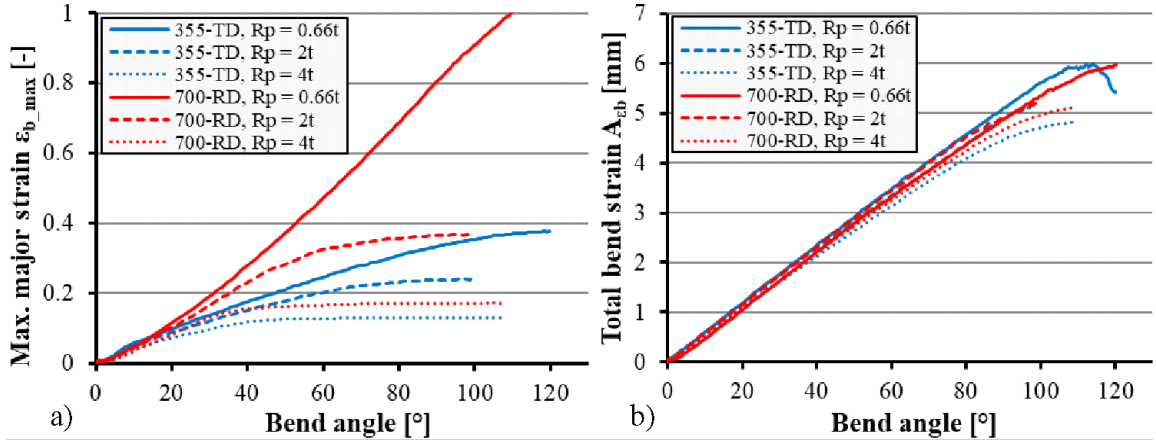

Fig. 4. Development of a) the peak strain and b) the total strain of St355 (TD) and St700 (RD), with punch radii of R_p = 0.66 t, R_p = 2 t, and R_p = 4 t.

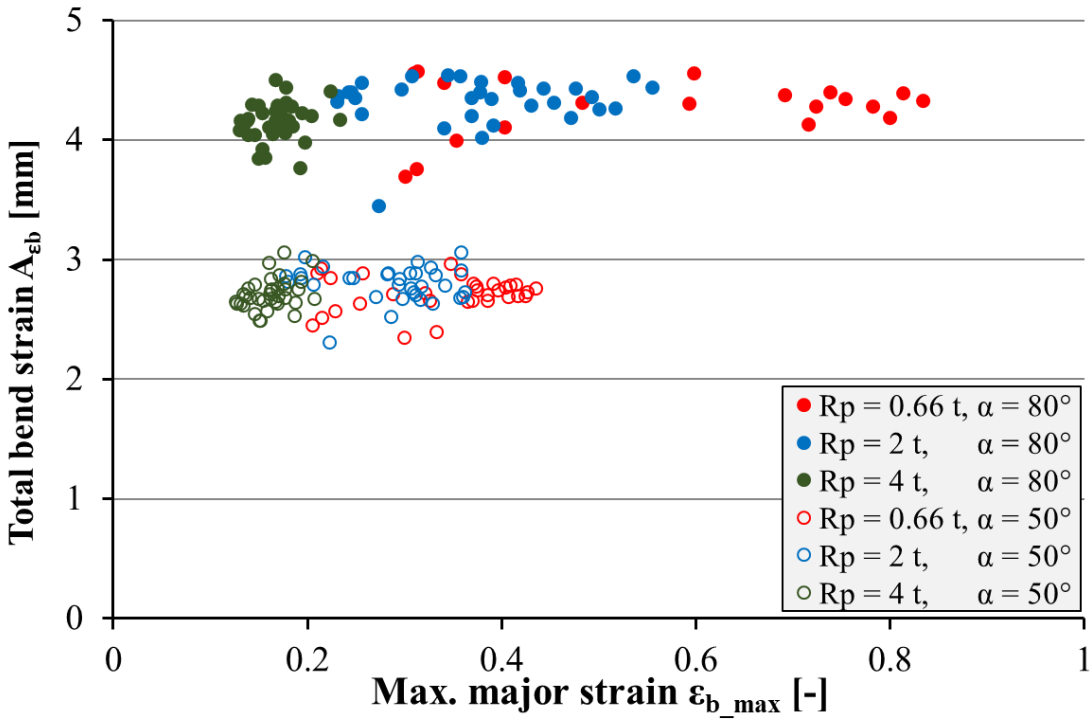

Fig. 5. Relationship between the total bend strain $A_{\varepsilon b}$ and the peak strain ε_{b_max}.

The total strain $A_{\varepsilon b}$ seems to be independent of the material properties, punch radius, the shape of the strain distribution or bend geometry. Assuming that the apparent stagnation after 80° is indeed caused by the limitations in the DIC field-of-view, the total strain seems to be a linear function of the bend angle. It should be possible to find an analytical solution for this relationship.

The parameters involved in this section are presented in Fig. 2. The bending angle α can be expressed as a sum of the rotation angles ϕ of the incremental arc lengths ds of the neutral axis, between the points a and b at the end of each flange, as follows:

$$\alpha = \int_a^b \frac{d\varphi(s)}{ds} ds \tag{1}$$

where s is an arc coordinate indicating the position on the neutral axis, and a and b are the end points of the neutral axis. The radius of the neutral axis R_n can also be expressed as

$$\frac{d\varphi}{ds} = \frac{1}{R_n}. \tag{2}$$

If the neutral axis is assumed to be positioned at the mid-thickness of the sheet, the strain on the outer surface ε_b can be given as

$$\varepsilon_b = \frac{t}{2R_n} \tag{3}$$

Combining Eq. 1, 2, and 3, the total strain on the outer bend surface (i.e., the strain distribution area) can be calculated as

$$A_{\varepsilon_b} = \int_a^b \varepsilon_b\,(s)\,ds = \int_a^b \frac{t}{2R_n}(s)\,ds = \frac{t}{2}\int_a^b \frac{1}{R_n}(s)\,ds = \frac{t}{2}\int_a^b \frac{d}{dS}\varphi\,(s)ds = \frac{\alpha t}{2} \tag{4}$$

The total strain $A_{\varepsilon b}$ seems to be a function of the bend angle and sheet thickness. If the total strain is constant for a given bend angle and sheet thickness, and all strain distributions in air bending are assumed to follow a known shape, e.g., a triangular function, the peak strain could be used to approximate the width of the strain distribution and the shape of the bent sheet. The approximate shape of the sheet could then be used for calculating the bend allowance and bend deduction, as well as approximating the effects of multi-breakage (loss of punch-sheet contact). Therefore, the peak strain ε_{b_max} at a given bend angle could be considered a decent stand-alone measure for the strain distribution. Furthermore, the effects of different material and tool parameters on the strain distribution development can then be investigated through simple linear regression, using the measured peak strain at a specific bend angle as the dependent variable.

In Fig. 6, the average total strains of all tests for each punch radius are plotted against the bend angle. The analytical total strain, calculated using Eq. 4, is included as a reference. Again, the total strain increases linearly for all punch radii until around 80°, after which a stagnation can be seen, presumably due to the limits of the DIC field-of-view (FOV). Although the analytical approximations are mostly within the standard deviation of the measured average values, the approximation seems to slightly underestimate the total strains. This could be due to the assumption of a fixed neutral axis in the analytical solution. If the neutral axis shifts towards the inside surface of the bend, the total strain on the outer surface will increase. For more precise analytical solutions and approximations in future works, the effects of the neutral axis shift could be considered.

Other factors that affect these measurements include the potential errors in the bend angle calculation, variation in sheet thickness and the loss of data due to fractures. If the ISO 7438 bend angle calculation overestimates the real bend angle, as was found by Cheong et al. [10], this would cause a downward bias to the measured $A_{\varepsilon b} - \alpha$ curves. However, the calculation of bend angle is hugely dependent on the tool geometry, so the previous findings may not necessarily apply for the geometry used in this study. Nevertheless, the calculation error of the bend angle introduces an additional unknown variable, and direct measurement of the bend angle would be preferable in future works.

As the total strain seems to be directly proportional to the sheet thickness, variations in sheet thickness will increase the scatter in the measured total strain. For more precise measurements and predictions, the sheet thickness variation should also be taken into account.

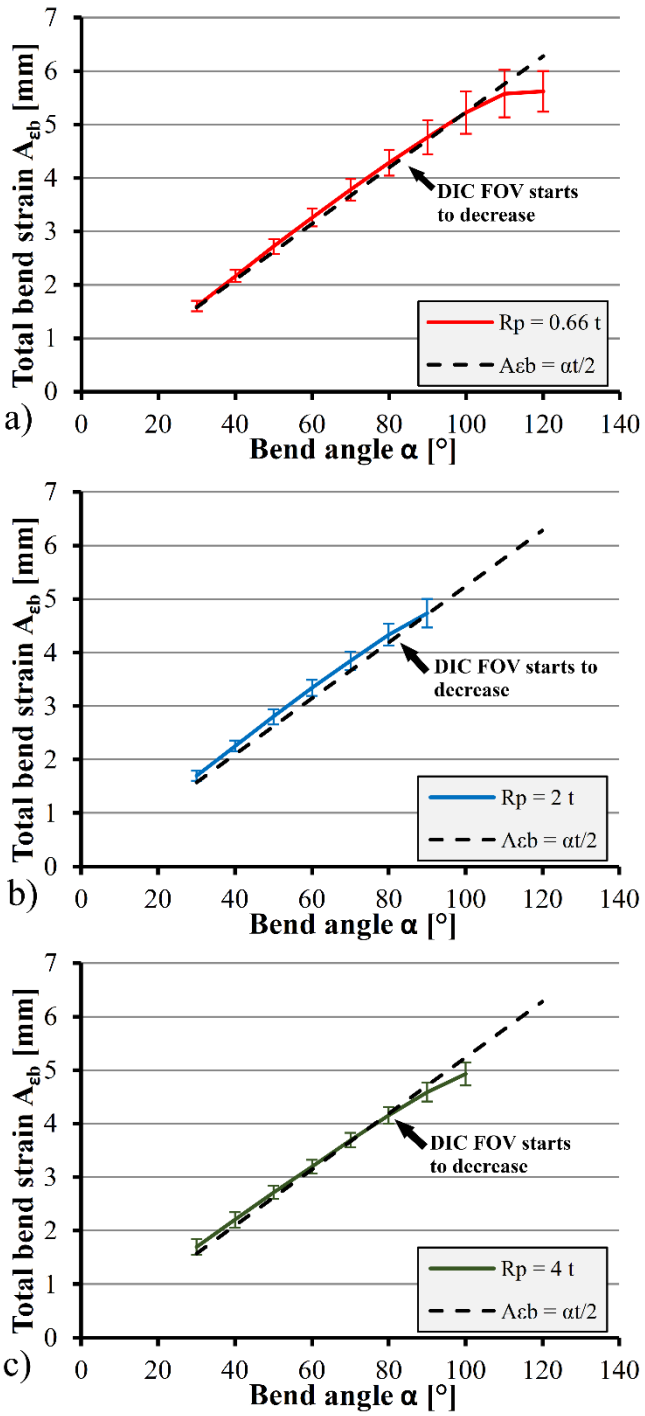

Fig. 6. Average total strain $A_{\varepsilon b}$, measured from bends with punch radius of a) R_p = 0.66 t, b) R_p = 2 t and c) R_p = 4 t. Analytical total strain is included as a reference, calculated as $A_{\varepsilon b} = \alpha t/2$, where t = 6 mm and α is the bend angle in radians.

Out of the 36 specimens tested with the punch radius R_p = 0.66 t, 16 fractured before 80° bend angle. For R_p = 2 t, four specimens fractured before 80°. As the tests were stopped at fracture, no data was gathered from these specimens after their fracture. Consequently, the sample size is decreased for the smaller punches and larger angles, meaning that the remaining specimens have more weight on the results. This increases the effect of random variation on the results, and could potentially introduce a bias, as only the specimens with the greatest ductility remain.

Part of the scatter and deviations in the total bend strain $A_{\varepsilon b}$, seen in Figs. 5 and 6 could be reduced if the DIC strain measurement setup and procedures were optimised for capturing the entire strain distribution. The setup and procedures used in this study were developed prioritizing the measurement of the peak strain, leading to increased noise and loss of data around the edges of the strain distributions. This could also be refined in future works.

Summary

The aim of this study was to characterize nine thermomechanically rolled steel grades with various strengths and ductility properties by means of their bendability properties using three different punch radii. The strain distributions on the outer curvature are measured throughout the test with a DIC system. The target was to understand and determine the relationships between the strain distribution, peak strain and total strain in air bending. The main observations and conclusions of the work can be summarized as follows:

- The strain distribution and peak strain had no measurable effect on the total strain on the outside surface. The total strain was found to grow at a similar rate throughout the test regardless of the punch radius or material properties.
- The total strain on the outside surface of the bend seems to be a function of the bend angle and sheet thickness. A decent approximation for the total strain was achieved with an analytical formula.
- The peak strain could be considered a decent stand-alone value for describing or approximating the strain distribution for a certain bend angle and sheet thickness. Possible use cases and benefits of such an approximation are discussed. These could include estimating the bend shape, multi-breakage, bend allowance and bend deduction, as well as allowing the use of simple linear regression for investigating the effects of certain material and tool parameters on the strain distribution development.

Acknowledgments

Financial assistance of the Business Finland, project FOSSA– Fossil-Free Steel Applications, is acknowledged.

References

[1] A.-P. Pokka, A.-M. Arola, A. Kaijalainen, V. Kesti, J. Larkiola, Strain distribution during air bending of ultra-high strength steels, ESAFORM 2021 (2021). https://doi.org/10.25518/esaform21.2509

[2] S.D. Benson, Press Brake Technology: A Guide to precision sheet metal bending, Society of Manufacturing Engineers, Dearborn, Michigan, 1997.

[3] V. Vorkov, R. Aerens, D. Vandepitte, J.R. Duflou, The Multi-Breakage Phenomenon in Air Bending Process, Key Eng. Mater. 611–612 (2014) 1047-1053. https://doi.org/10.4028/www.scientific.net/KEM.611-612.1047

[4] A. Väisänen, K. Mäntyjärvi, J.A. Karjalainen, Bendability of Ultra-High-Strength Steel, Key Eng. Mater. 410–411 (2009) 611-620. https://doi.org/10.4028/www.scientific.net/KEM.410-411.611

[5] J. Heikkala, A. Väisänen, Usability Testing of Ultra High-Strength Steels, Proc. ASME 2012 11th Biennial Conference on Engineering Systems Design and Analysis 4 (2012) 163-173. https://doi.org/10.1115/ESDA2012-82770

[6] V. Kesti, A. Kaijalainen, A. Väisänen, A. Järvenpää, A. Määttä, A.-M. Arola, K. Mäntyjärvi, R. Ruoppa, Bendability and Microstructure of direct quenched Optim® 960QC, Mater. Sci. Forum 783-786 (2014) 818-824. https://doi.org/10.4028/www.scientific.net/MSF.783-786.818

[7] A.-M. Arola, V. Kesti, R. Ruoppa, The effect of punch radius on the deformation of ultra-high strength steel in bending, Key Eng. Mater. 639 (2015) 139-146.

[8] L. Wagner, H. Schauer, H. Pauli, J. Hinterdorfer, Improved bendability characterization of UHSS sheets, IOP Conf. Ser. Mater. Sci. Eng. 651 (2019) 012019. https://doi.org/10.1088/1757-899X/651/1/012019
[9] M. Kaupper, M. Merklein, Bendability of advanced high strength steels - A new evaluation procedure, CIRP Ann. - Manuf. Technol. 62 (2013) 247-250. https://doi.org/10.1016/j.cirp.2013.03.049
[10] K. Cheong, K. Omer, C. Butcher, R. George, J. Dykeman, Evaluation of the VDA 238-100 Tight Radius Bending Test using Digital Image Correlation Strain Measurement, J. Phys. Conf. Ser. 896 (2017) 12075. https://doi.org/10.1088/1742-6596/896/1/012075
[11] A.-M. Arola, A. Kaijalainen, V. Kesti, A.-P. Pokka, J. Larkiola, Digital image correlation and optical strain measuring in bendability assessment of ultra-high strength structural steels, Procedia Manuf. 29 (2019) 398-405. https://doi.org/10.1016/j.promfg.2019.02.154
[12] S. Gothivarekar, S. Coppieters, A. Van de Velde, D. Debruyne, Advanced FE model validation of cold-forming process using DIC: Air bending of high strength steel, Int. J. Mater. Form. 13 (2020) 409-421. https://doi.org/10.1007/s12289-020-01536-1
[13] R. Ruoppa, R. Toppila, V. Kesti, A. Arola, Bendability tests for ultra-high-strength steels with optical strain analysis and prediction of bending force, Proc. METNET Seminar 2014 Moscow (2014) 68-78.
[14] C. Suppan, T. Hebesberger, A. Pichler, J. Rehrl, O. Kolednik, On the microstructure control of the bendability of advanced high strength steels, Mater. Sci. Eng. A 735 (2018) 89-98. https://doi.org/10.1016/j.msea.2018.07.080
[15] SFS-EN ISO 7438:2016: Metallic materials – Bend test.